Role of sodium channel subtype in action potential generation by neocortical pyramidal neurons

Efrat Katz[a,1], Ohad Stoler[b,c,1], Anja Scheller[d,1], Yana Khrapunsky[b,c], Sandra Goebbels[e], Frank Kirchhoff[d], Michael J. Gutnick[a], Fred Wolf[f,g], and Ilya A. Fleidervish[b,c,2]

[a]Koret School of Veterinary Medicine, Hebrew University of Jerusalem, Rehovot 7610001, Israel; [b]Department of Physiology and Cell Biology, Faculty of Health Sciences, Ben-Gurion University of the Negev, Beer Sheva 8410501, Israel; [c]Zlotowski Center for Neuroscience, Ben-Gurion University of the Negev, Beer Sheva 8410501, Israel; [d]Department of Molecular Physiology, Center for Integrative Physiology and Molecular Medicine, University of Saarland, 66421 Homburg, Germany; [e]Department of Neurogenetics, Max Planck Institute of Experimental Medicine, 37075 Göttingen, Germany; [f]Research Group of Theoretical Neurophysics, Max Planck Institute for Dynamics and Self-Organization, 37077 Göttingen, Germany; and [g]Bernstein Center for Computational Neuroscience and Faculty of Physics, University of 37077 Göttingen, Germany

Edited by Bruce P. Bean, Harvard Medical School, Boston, MA, and approved June 14, 2018 (received for review November 24, 2017)

Neocortical pyramidal neurons express several distinct subtypes of voltage-gated Na^+ channels. In mature cells, $Na_v1.6$ is the dominant channel subtype in the axon initial segment (AIS) as well as in the nodes of Ranvier. Action potentials (APs) are initiated in the AIS, and it has been proposed that the high excitability of this region is related to the unique characteristics of the $Na_v1.6$ channel. Knockout or loss-of-function mutation of the *Scn8a* gene is generally lethal early in life because of the importance of this subtype in noncortical regions of the nervous system. Using the Cre/loxP system, we selectively deleted $Na_v1.6$ in excitatory neurons of the forebrain and characterized the excitability of $Na_v1.6$-deficient layer 5 pyramidal neurons by patch-clamp and Na^+ and Ca^{2+} imaging recordings. We now report that, in the absence of $Na_v1.6$ expression, the AIS is occupied by $Na_v1.2$ channels. However, APs are generated in the AIS, and differences in AP propagation to soma and dendrites are minimal. Moreover, the channels that are expressed in the AIS still show a clear hyperpolarizing shift in voltage dependence of activation, compared with somatic channels. The only major difference between $Na_v1.6$-null and wild-type neurons was a strong reduction in persistent sodium current. We propose that the molecular environment of the AIS confers properties on whatever Na channel subtype is present and that some other benefit must be conferred by the selective axonal presence of the $Na_v1.6$ channel.

axon initial segment | conditional knockout | action potential | $Na_v1.6$ channel | Na^+ flux

Operation of neuronal networks relies on the ability of neurons to generate complex electrochemical signals, called action potentials (APs) (1). A precise characterization of the mechanisms underlying this signaling is key to understanding sensory processing, motor control, neuroplasticity, and other brain functions. The mechanism of AP generation critically depends on the distribution and properties of voltage-gated Na^+ channels within the cellular compartment where APs initiate. Thus, determining these channel properties, including their molecular composition and their activation and inactivation kinetics within the spike trigger zone, has been a focus of intense research over the past decade (2, 3).

Central neurons of mammals express four genes (*Scn1a*–*Scn3a* and *Scn8a*) encoding Na^+ channels α-subunits $Na_v1.1$–$Na_v1.3$ and $Na_v1.6$ (4). Although the details of their cellular and subcellular distribution are incompletely understood, it is widely believed that the distinct channels are specifically expressed and targeted and possess unique functional characteristics. In many central neurons, the AP trigger zone, which is located in the distal portion of the axon initial segment (AIS), contains almost exclusively $Na_v1.6$ channels (5–8). This fact makes it tempting to believe that it is the presence of the $Na_v1.6$ channels in the distal AIS that makes it the preferable site for AP initiation. This idea is supported by the finding that heterologously expressed $Na_v1.6$ channels activate at lower voltages than other channel subtypes (9) (but see refs. 10 and 11) and have a higher propensity to generate a noninactivating persistent Na^+ current (I_{NaP}) (9, 11, 12). Axonal Na^+ channels within the trigger zone have also been shown to activate at lower voltages (6, 13, 14) and to generate more I_{NaP} (15–17) than those in soma and dendrites. Compartmental modeling predicts that the threshold for spike initiation is influenced by Na^+ channel voltage dependence (6, 13) and by I_{NaP} magnitude (18, 19). Therefore, APs would be strongly biased to initiate at the site of the greatest density of low-threshold channels that generate I_{NaP} if other conditions are similar. These arguments are indirect, however. Also, compartmental modeling shows that special low-threshold gating of sodium channels is not necessary for the preferential initiation of action potentials in the distal AIS, which can be predicted by models with a single sodium conductance of uniform gating properties provided there is a higher density in the AIS (20–23).

One direct strategy to address the role of $Na_v1.6$ channels is the suppression of their expression to test the consequences of channel loss. Implementation of this approach for studying cortical neurons, circuits, and cortex-related behavior, however, has been impeded by the short life span of $Na_v1.6$ null mice; these mice die at the age of 21–24 d (24), long before $Na_v1.6$ expression in the forebrain reaches the adult level (25). We therefore used a Cre/loxP approach to selectively ablate the encoding *Scn8a* gene in excitatory neurons of the forebrain,

Significance

Under most conditions cortical pyramidal neurons are strongly biased to initiate action potentials in the distal part of the axon initial segment (AIS) rather than in the dendrites, where the excitatory postsynaptic potential amplitude is largest. This feature is widely attributed to the axonal presence of the low-threshold Na^+ channel subtype $Na_v1.6$. Here, using electrical and high-speed Na^+ imaging recordings from $Na_v1.6$ null pyramidal neurons, we demonstrate that the presence of this subunit is neither critical for positioning the spike initiation site within the AIS nor for the spike backpropagation to the dendrites. We also find that one of the most important features of axonal Na^+ channel kinetics, the lower activation threshold, is not entirely dependent on the Na^+ channel subtype.

Author contributions: F.K., M.J.G., F.W., and I.A.F. designed research; E.K., O.S., A.S., Y.K., and I.A.F. performed research; S.G. contributed new reagents/analytic tools; E.K., O.S., A.S., Y.K., F.K., M.J.G., F.W., and I.A.F. analyzed data; and A.S., F.K., M.J.G., F.W., and I.A.F. wrote the paper.

The authors declare no conflict of interest.

This article is a PNAS Direct Submission.

[1]E.K., O.S., and A.S. contributed equally to this work.

[2]To whom correspondence should be addressed. Email: ilya@bgu.ac.il.

This article contains supporting information online at www.pnas.org/lookup/suppl/doi:10.1073/pnas.1720493115/-/DCSupplemental.

Published online July 10, 2018.

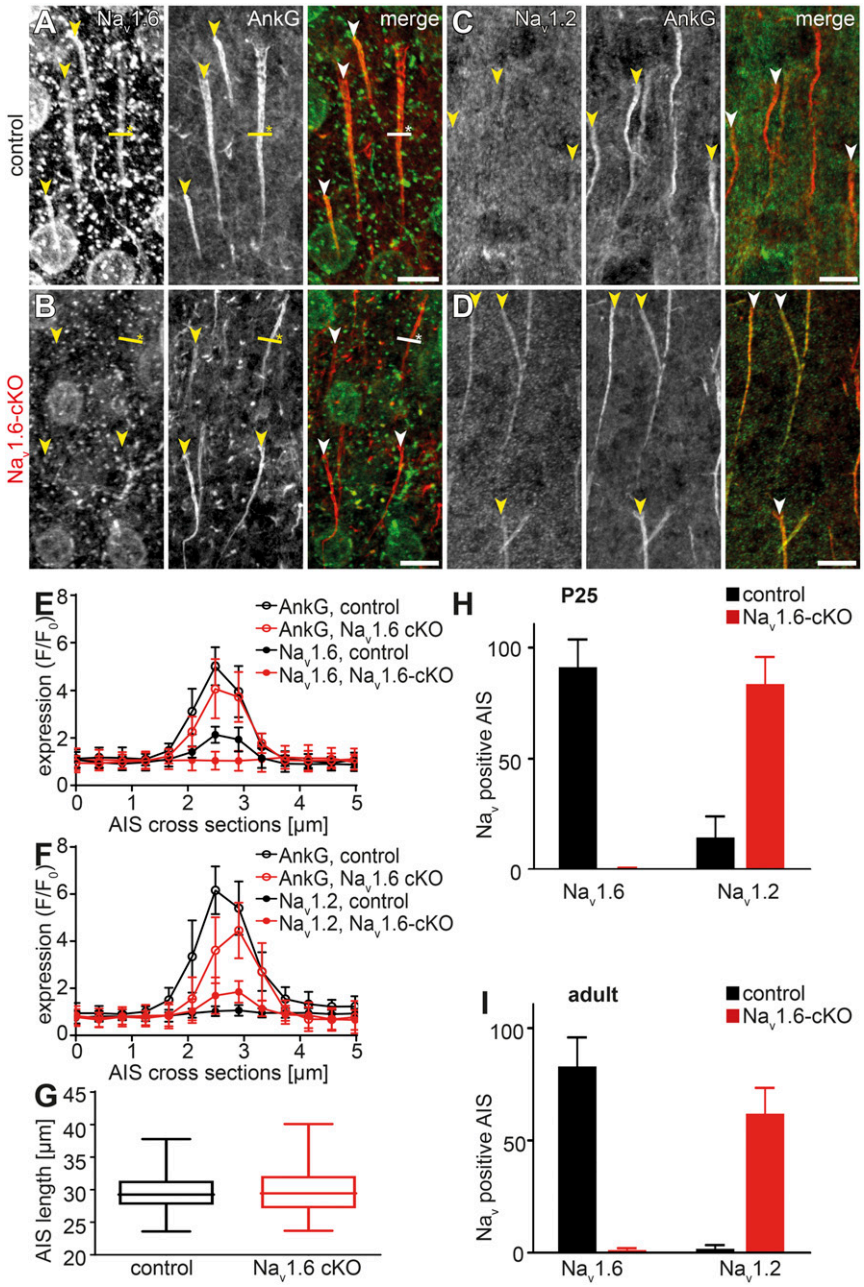

Fig. 1. Expression of Na^+ channel subtypes at the AIS of L5 pyramidal neurons in control and $Na_v1.6$-cKO mice. (*A–D*) Confocal micrographs of $Na_v1.6$ (*A* and *B*), $Na_v1.2$ (*C* and *D*), and AnkG immunostains in the layer 5 cortical sections of adult control (*A* and *C*) and $Na_v1.6$-cKO (*B* and *D*) mice. Arrowheads indicate the proximal boundary of the AnkG-labeled AIS. Yellow lines with asterisks indicate the cross-section positions analyzed in *E* and *F*. $Na_v1.6$ channels are present over the entire AIS length in neurons of adult control mice, while they are absent in $Na_v1.6$ cKO mice (*A* and *B*, merged images). $Na_v1.2$ channels are barely detectable in AISs of control neurons, but strongly up-regulated in the $Na_v1.6$-deficient neurons (*C* and *D*, merged images). (Scale bars, 10 μm.) (*E* and *F*) Sections across the AISs (2.5 μm on both sides) were used to quantify $Na_v1.6$, $Na_v1.2$, and AnkG expression in adult mice (analyzed as F/F_0). While AnkG expression remained constant in control (black) and $Na_v1.6$-deficient (red) AISs, $Na_v1.2$ is present in the $Na_v1.6$-cKO AISs at approximately the same levels as $Na_v1.6$ in control AISs. (*G*) Analysis of AIS length as measured by AnkG expression did not reveal significant difference between $Na_v1.6$-cKO (red) and control (black) neurons. (*H* and *I*) Fractions of $Na_v1.6$- and $Na_v1.2$-positive AISs of control (black) and $Na_v1.6$-cKO (red) neurons in young (P25, *H*) and adult (P60, *I*) mice. Note that the $Na_v1.6$ deficiency is almost completely compensated for by $Na_v1.2$.

including cortical pyramidal cells, using the well-established NEX-Cre knockin mouse line (26). While previous studies were based on somatic electrical recordings alone, in the present work we used a combination of electrical current- and voltage-clamp recordings with direct measurements of axonal Na^+ fluxes using high-speed fluorescence imaging (17, 27).

We found that the L5 pyramidal cell axons of the adult $NEX^{cre/wt}/Scn8a^{fl/fl}$ mice [referred to hereafter as $Na_v1.6$ conditional knockout (cKO)] are deficient in $Na_v1.6$ channels, which apparently fail to replace the $Na_v1.2$ channels in a course of postnatal maturation (28). Surprisingly, APs elicited in cortical pyramidal neurons from $Na_v1.6$-cKO mice had a rapid onset and biphasic upstroke, indicating that $Na_v1.6$ is not critically important for positioning the AP initiation site in the AIS. Imaging experiments revealed that Na^+ fluxes in the AIS of L5 cortical pyramidal neurons associated with single or multiple APs were not significantly different in

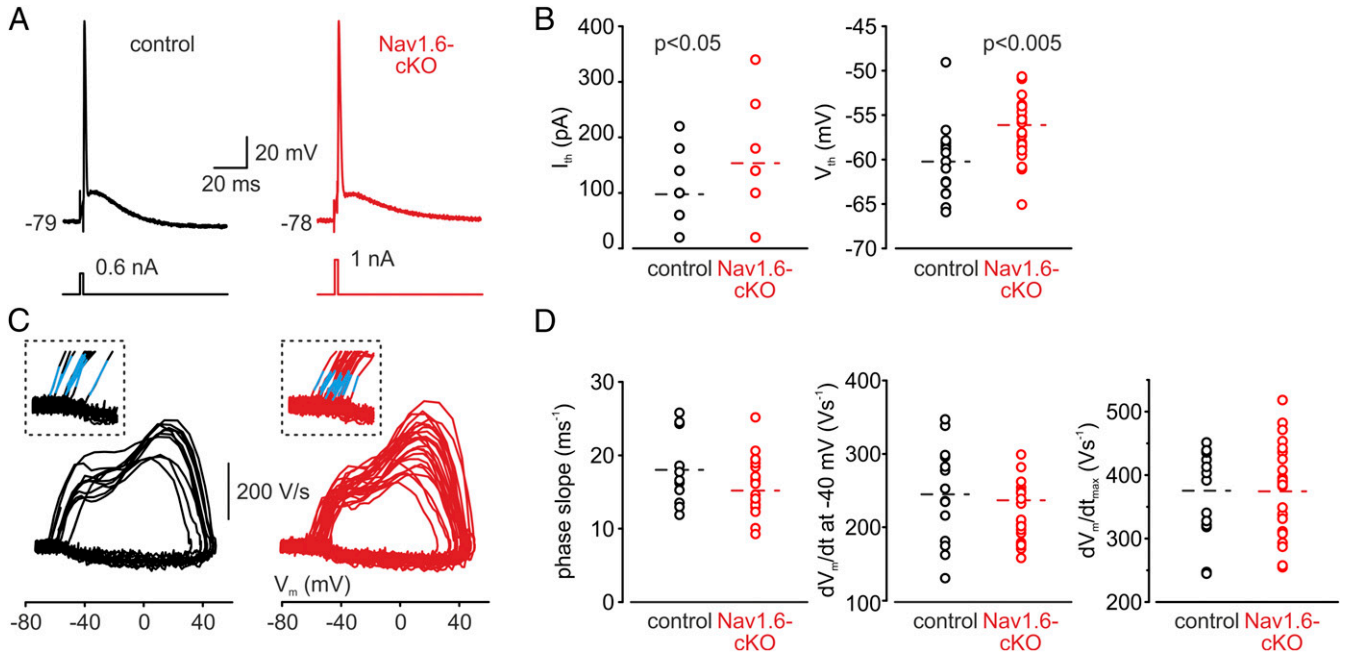

Fig. 2. Threshold for AP generation is higher in $Na_v1.6$-cKO neurons. (*A*) Single APs elicited in control (black trace) and $Na_v1.6$-cKO (red trace) pyramidal neurons by brief (2 ms), just-suprathreshold current pulses. (*B*) Current threshold is significantly increased and voltage threshold is depolarized in cKO neurons. Dots represent the values for the current and voltage thresholds measured in individual control (black) and cKO (red) cells. The dashed lines indicate the mean values. (*C*) Phase plots (*dV/dt* vs. *V*) of AP upstroke in control (black, $n = 14$) and cKO (red, $n = 23$) neurons are invariably biphasic. (*Inset*) Expanded view of the initial phase of the AP upstroke, with superimposed linear fit (blue). (*D*) The temporal dynamics of spike upstroke is preserved in $Na_v1.6$-cKO neurons. Dots represent the values for the slope of the initial rise (*Left*), AP rate of rise at −40 mV (*Middle*), and dV/dt_{max} (*Right*) in control (black) and cKO (red) neurons.

$Na_v1.6$-cKO and control animals. Although the magnitude of the axonal persistent Na^+ current in $Na_v1.6$-cKO mice was reduced, its activation was still leftward shifted compared with the persistent current recorded in the soma, indicating that the axo-somatic difference in I_{NaP} activation voltage is not solely dependent on the difference in Na^+ channel subtype.

Results

Cell-specific conditional *Scn8a* knockout mice were generated by crossbreeding NEX-Cre (Neuro D6) mice (26) with floxed *Scn8a* mice (29). Since NEX promoter activity is largely restricted to the principal excitatory neurons of the forebrain (26), including L5 pyramidal neurons, Cre DNA recombinase expression and *Scn8a* gene inactivation in $NEX^{cre/wt}$-$Scn8a^{fl/fl}$ animals is expected to be confined to this neuronal population. Indeed, unlike mice with nonconditional *Scn8a* ablation, that do not live more than 3 wk (24), the homozygous cell-specific conditional knockout ($Na_v1.6$-cKO) mice had a normal life span and did not developed any obvious brain or behavioral abnormalities.

To characterize the subcellular distribution of Na^+ channel subtypes in L5 pyramidal neurons, cortical sections from 1-mo-old male control and $Na_v1.6$-cKO mice were stained with $Na_v1.2$ and $Na_v1.6$ antibodies (Fig. 1 *A–D*). AISs were identified by costaining of the cytoskeletal protein, ankyrin-G (AnkG) that is present only in the AIS and in nodes of Ranvier of myelinated cortical fibers (30, 31). Quantitative evaluation of the immunofluorescent signals revealed a complete loss of $Na_v1.6$ expression in the AISs of the $Na_v1.6$-cKO neurons. Interestingly, this loss was compensated for by complementary expression of $Na_v1.2$ channels (Fig. 1 *E* and *F*). This subunit exchange, however, did not affect the gross structural organization of the AIS as no differences in the pattern of AnkG expression could be detected in $Na_v1.6$-cKO and control neurons. AIS length, measured by the immunofluorescent signal for AnkG, revealed no significant difference (29.6 ± 2.7 μm in control mice vs. 30.0 ± 3.7 μm in cKO, $P = 0.7237$, Mann–Whitney *U* test, Fig. 1*G*). Measuring AIS length using the functionally more relevant Na_v immunofluorescence, in both $Na_v1.6$-cKO and control neurons, produced highly variable results, because of low signal intensity at the distal AIS.

In young control mice (P25), most AnkG-positive AISs of L5 neurons ($n = 423$) contained only $Na_v1.6$ channels (91.3 ± 12.3%), whereas $Na_v1.2$ presence was detected in a few cells (14.4 ± 9.5%, Fig. 1*H*). In sections from brains of $Na_v1.6$-cKO mice, however, most of the analyzed AISs ($n = 210$) were $Na_v1.2$-positive (83.7 ± 12.0%). At this age, only 0.32 ± 0.45% of AISs expressed $Na_v1.6$. In adult control mice [postnatal day 60 (P60)], 82.9 ± 13.0% of all AISs ($n = 3385$) were $Na_v1.6$-positive while only 1.8 ± 1.6% were positive for $Na_v1.2$. In adult $Na_v1.6$-cKO mice, however, only 1.26 ± 0.8% of all AnkG-positive AISs ($n = 3913$) contained $Na_v1.6$, while the large majority of the AISs (61.9 ± 11.5%) contained $Na_v1.2$ (Fig. 1*I*). We concluded that failure of up-regulation of $Na_v1.6$ expression during the maturation of L5 pyramidal cells results in retention of the juvenile channel subtype, $Na_v1.2$, in their axons.

$Na_v1.6$ Deficiency Has a Minor Effect on AIS Spike Initiation. To characterize the functional consequences of the $Na_v1.6$ deficiency, whole-cell somatic current-clamp recordings were obtained from large L5 pyramidal neurons in coronal brain slices from 4- to 5-wk-old $Na_v1.6$-cKO mice and control littermates (Fig. 2*A*). Since damage to the proximal axon during preparation of the tissue slice might significantly influence firing properties of pyramidal cells, we made sure that the axons were preserved by filling the cells with the fluorescent Na^+ indicator sodium-binding benzofuran isophthalate (SBFI) and directly visualizing the thin neuronal processes emerging from the cell body. Axons were distinguished by their distinctive shape and by the magnitude of their spike-elicited Na^+ transients (17). Data from cells in which the axons

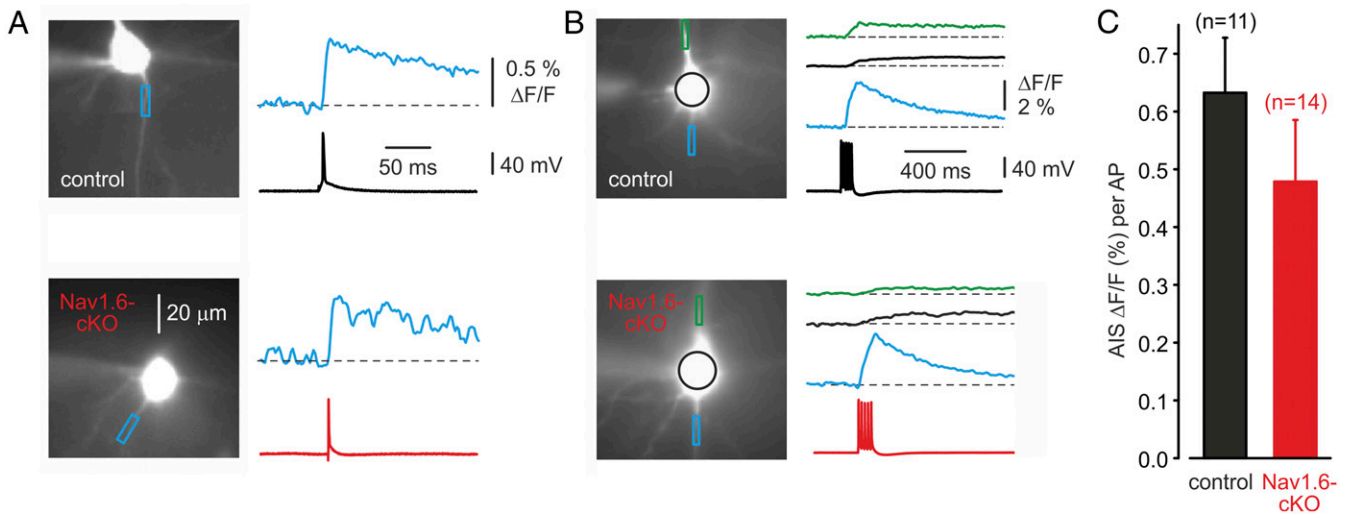

Fig. 3. AP elicited $[Na^+]_i$ elevations in control and $Na_v1.6$-cKO neurons. (*A*) $[Na^+]_i$ elevations elicited in AIS of the control (*Upper* traces) and cKO (*Lower* traces) cells by a single AP. (*B*) $[Na^+]_i$ changes associated with a train of five spikes elicited by current pulses at 20 Hz. Note that the magnitudes, spatial distributions, and time courses of the changes were similar for control and cKO neurons. Colors of traces indicate regions of interest in apical dendrite, soma, and AIS. (*C*) The mean peak amplitude of the AIS Na^+ transients evoked by a single AP does not differ between the control ($n = 11$) and cKO ($n = 14$) neurons ($P > 0.05$).

were cut at a distance of less than 150 μm from the soma were not included in the analysis. The resting membrane potential and passive membrane characteristics of $Na_v1.6$-cKO neurons were not significantly different from those of controls (*SI Appendix*, Table S1). Current and voltage spike thresholds, however, were slightly elevated in the $Na_v1.6$-cKO neurons compared with controls (Fig. 2*B*).

If the presence of low-threshold $Na_v1.6$ channels in distal AIS was indeed critical for AP initiation (6, 13, 14), loss of these channels would be expected to exert a significant change in the pattern of AP generation in response to orthodromic stimuli. Therefore, we compared the phase plots of somatically recorded APs in L5 pyramidal neurons from $Na_v1.6$-cKO and control mice (Fig. 2*C*). The phase plot of the upstroke of the somatic spike describes the rate of change of the membrane potential (dV_m/dt) as a function of the instantaneous membrane potential (V_m). It is typically biphasic, with the first phase generated predominately by the lateral current from the AIS, and the second phase generated by the local, somatic Na^+ channels (6, 32). Surprisingly, all features of the AP dynamics, including biphasic shape, rapid onset, voltage, and time dependence of the rate of rise were preserved in $Na_v1.6$-cKO mice (Fig. 2*D*). Thus, the role of $Na_v1.6$ channels in creating conditions for AP initiation in the distal AIS seems not to be critical, as deletion of these channels is almost completely compensated for by the retained $Na_v1.2$ channels.

Pattern of AP-Associated AIS Na^+ Influx Is Not Altered by $Na_v1.6$ Deletion. We considered the possibility that the somatic AP dynamics might be preserved in $Na_v1.6$-cKO neurons because of some compensatory change in AIS length or position relative to the cell body (33, 34). Morphometric analysis of the AnkG immunosignal, however, revealed a difference in neither AIS position nor in its mean length (Fig. 1*G*). To characterize the Na^+ channel distribution and density in proximal axons more directly, neurons were filled with the Na^+ indicator SBFI. We first focused on Na^+ signals elicited by single APs, as the peak amplitude of these signals should be almost unaffected by lateral diffusion and therefore can be used as a measure of local Na^+ entry (17, 27). Single APs elicited rapidly rising, fast-decaying Na^+ transients that were prominent only in the AIS and were poorly or not at all detectable in soma and dendrites (17, 27). Measurements of peak amplitude of the averaged ΔF/F transients over the 20 μm of distal AIS length revealed no significant difference between the two groups of neurons (Fig. 3*A*, 0.50 ± 0.20%, $n = 4$, $Na_v1.6$-cKO neurons vs. 0.70 ± 0.14%, $n = 4$ control neurons, $P > 0.05$). Comparison of the axonal Na^+ transients elicited by trains of five APs, each evoked by a 2-ms-long current step, yielded qualitatively similar results (Fig. 3 *B* and *C*), with no significant difference in per spike Na^+ elevation between $Na_v1.6$-cKO and control neurons. Trains of five spikes also elicited Na^+ elevations in the somata and proximal apical dendrites of $Na_v1.6$-cKO and control cells. These transients, which were presumably generated by activation of the prevailing somato-dendritic channel subtype $Na_v1.2$ (6), were not affected by the $Na_v1.6$ deletion.

Since the comparison of ΔF/F proportional to spike evoked $[Na^+]_i$ elevations is based on the assumption that the axonal surface-to-volume ratio, tissue autofluorescence, and other parameters are unchanged, we also compared the axo-somatic ΔF ratios in $Na_v1.6$-cKO and control neurons. Peak ΔF, a parameter that is roughly proportional to the Na^+ influx per unit of membrane area (17, 27), was measured in the soma and the AIS following trains of five APs evoked by brief current steps (Fig. 4*A*). The axo-somatic ΔF ratio in the $Na_v1.6$-cKO neurons (1.91 ± 0.32, $n = 10$) was not significantly different from the ratio in control cells (2.65 ± 0.63, $n = 9$, $P > 0.05$) (Fig. 4*B*).

$Na_v1.6$ Deficiency Has a Minor Effect on Repetitive Spike Firing and Dendritic Backpropagation. We next sought to determine whether the $Na_v1.6$ channel loss would affect the ability of L5 neurons to fire repetitively during prolonged depolarizing current pulses (Fig. 5*A*). Under this stimulation protocol, most control and $Na_v1.6$-cKO neurons were identified as "regular-spiking" cells (35). In the rare instances where cells exhibited an "intrinsic burster" firing pattern, they were not included in the present analysis. When depolarized by prolonged, suprathreshold current pulses of incrementing amplitude, both control and $Na_v1.6$-cKO neurons generated trains of APs with progressively increasing frequency. The frequency–current (F-I) characteristic of $Na_v1.6$-cKO neurons, constructed by plotting the mean instantaneous AP frequency as a function of depolarizing current pulse amplitude (Fig. 5*B*), was displaced to the right compared

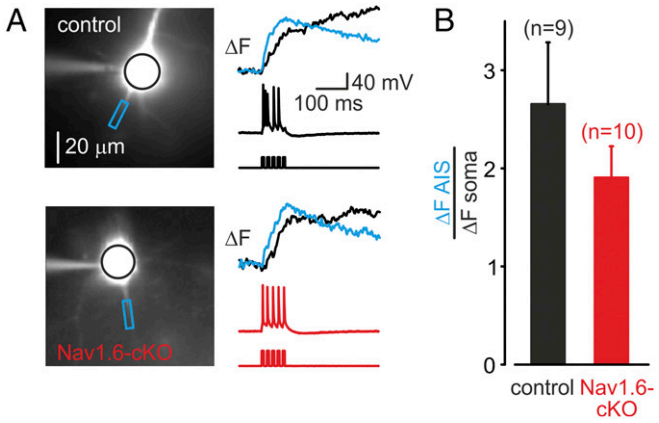

Fig. 4. AIS:soma ratio of AP-elicited Na^+ flux does not differ between control and cKO neurons. (*A*) Representative somatic (black) and AIS (blue) ΔF transients elicited by trains of five APs at 20 Hz in control and cKO neurons. (*B*) The mean ratio of the AIS and somatic peak amplitude of the ΔF transients evoked by trains of five APs does not differ between control (n = 9) and cKO (n = 10) neurons ($P > 0.05$).

with controls. However, the mean slope of the F-I relationship measured in the current range of 0.08–0.28 nA in $Na_v1.6$-cKO neurons (85.2 ± 6.2 Hz/nA, $n = 22$) was not significantly different from in controls (102.4 ± 9.3 Hz/nA, $n = 13$, $P = 0.12$).

Earlier studies (36, 37) have linked the ability of the central axons to generate high-frequency trains of APs with the rapid recovery of the axonal $Na_v1.6$ channels from inactivation. We therefore sought to compare the use-dependent changes in axonal Na^+ channel availability in $Na_v1.6$-cKO and control neurons during trains of APs elicited by brief current steps at 20 Hz. We found that, at this firing frequency, consecutive APs elicit progressively smaller Na^+ elevations in AIS of both control and $Na_v1.6$-cKO neurons (Fig. 6*A*). The use-dependent decline in the amplitude of ΔF/F transients underwent a similar time course in cKO and control cells (Fig. 6 *B* and *C*), indicating that there was little or no difference in reactivation kinetics of the underlying Na^+ channels.

Using immunogold labeling Lorincz and Nusser (38) found low, but significant, densities of the $Na_v1.6$ channels in soma and dendrites of hippocampal pyramidal neurons. To determine whether the $Na_v1.6$ loss has an effect on active invasion of the dendritic tree by the repetitive APs (39), we loaded the control and cKO neurons with Ca^{2+} indicator Oregon Green BAPTA-1 (OGB-1, 50 μM) via the somatic whole-cell pipette for at least 40 min. In both $Na_v1.6$-cKO and control cells, Ca^{2+} transients elicited by single APs had a similar amplitude along the apical dendrite, whereas the amplitude of Ca^{2+} transients elicited by trains of APs at 20 Hz decreased significantly with distance from the soma (Fig. 7*A*, *Left*). In distal locations, the transients typically peaked after the first few APs and then declined, with only minor change in slope at the end of the train (39, 40), reflecting the activity-dependent decrease in AP amplitude due to slow inactivation of Na^+ channels (41). In both control and cKO neurons, Ca^{2+} transients elicited by spike trains at higher frequency (50 Hz, Fig. 7*A*, *Right*) were less prone to attenuate as a function of distance (42). Dendritic profiles of the mean $[Ca^{2+}]_i$ change following the spike train normalized to the amplitude of single-spike–evoked Ca^{2+} transients in 7 control (black circles) and in 11 $Na_v1.6$-cKO (red circles) neurons show a similar extent of distance-dependent attenuation during spike trains at 20 and 50 Hz ($P > 0.05$, Fig. 7*B*). We conclude that $Na_v1.6$ deletion has a minimal effect on the fidelity of spike backpropagation in the apical dendritic tree of L5 pyramidal cells.

Persistent Na^+ Current in the AIS Is Primarily Generated by $Na_v1.6$ Channels. To study the contribution of $Na_v1.6$ channels to I_{NaP}, we examined the changes in $[Na^+]_i$ generated by slow depolarizing voltage ramps under voltage clamp with pharmacologically blocked K^+ and Ca^{2+} conductances. The maximal amplitude of the I_{NaP} generated by a slow ramp in $Na_v1.6$-cKO neurons (329 ± 205 pA, $n = 7$) was significantly smaller than in control cells (642 ± 297 pA, $n = 6$) ($P < 0.05$) (Fig. 8*A*). Analysis of ramp-evoked AIS Na^+ transients revealed that the peak amplitude in $Na_v1.6$-cKO neurons (11.2 ± 1.7% ΔF/F, $n = 6$) was also reduced compared with control cells (6.3 ± 1.3%, $n = 6$, $P < 0.05$). Comparison of voltage dependence of the ramp-elicited Na^+ fluxes, however, revealed that, in both $Na_v1.6$-cKO and control cells, the activation of I_{NaP} at the AIS occurs at more negative potentials than somatic I_{NaP} (Fig. 8*B*). The AIS-soma differences in I_{NaP} onset voltage were not significantly different between the $Na_v1.6$-cKO and control neurons (−12.0 ± 2.1 mV, $n = 6$ vs. −11.2 ± 1.8 mV, $n = 6$, respectively, $P = 0.78$).

Discussion

$Na_v1.6$, the dominant Na^+ channel subtype in the AIS of mature neocortical pyramidal cells, is widely believed to play an essential role in positioning the AP initiation site within the proximal axon. Our evidence, however, demonstrates that the presence of this subunit is not critical. We also find that one of the most important features of the behavior of axonal Na^+ channels, the leftward shift of their activation threshold (6, 13, 14), is not entirely dependent on the Na^+ channel subtype. Instead, it probably reflects local protein–protein interactions.

In contrast with previous studies in rat and human cortex (6, 8), we found that the large majority of AISs of pyramidal neurons in adult control mice is $Na_v1.2$ immuno-negative, whereas the AISs of the adult $Na_v1.6$-cKO neurons are almost exclusively populated by this channel subtype. The reason for this discrepancy remains unclear. It may reflect the species or age difference or pathological alterations in human tissue samples. Highly sensitive immunogold labeling (38) revealed low, but significant, densities of $Na_v1.6$ channels in soma and apical dendrites of control pyramidal neurons. Uncompensated loss of these channels in $Na_v1.6$-cKO cells would be expected to reduce dendritic excitability. Our evidence (Fig. 7) that $Na_v1.6$ deletion has no obvious effect on the fidelity of spike backpropagation indicates that the dendritic $Na_v1.6$ loss is compensated for by expression of

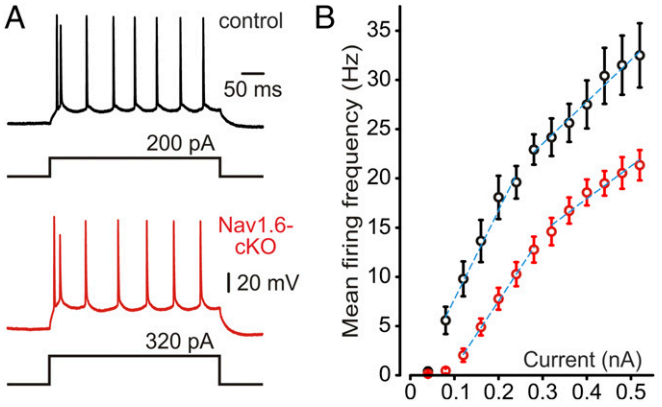

Fig. 5. Input/output gain is not altered in $Na_v1.6$-cKO neurons. (*A*) Repetitive firing elicited by prolonged current pulses in representative control and cKO neurons. Note that firing patterns are similar, but more current is required to achieve the same frequency in cKO neurons. (*B*) F-I relationships of neurons from control (black circles) and cKO (red circles) mice. Blue dashed lines represent the linear fits for nearly linear portions of the F-I relationships.

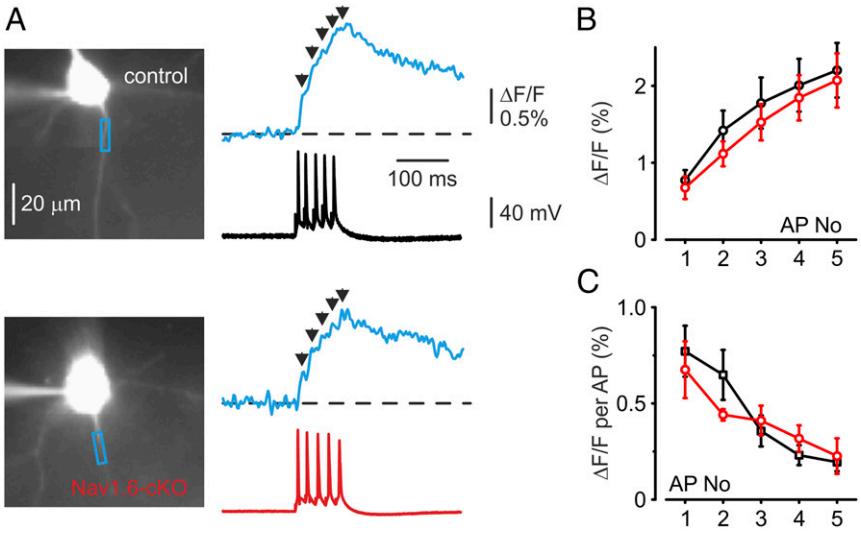

Fig. 6. Kinetics of use-dependent attenuation of the AIS Na^+ fluxes is not affected by the $Na_v1.6$ deletion. (*A*) Representative recordings of changes in AIS $[Na^+]_i$ during a train of five APs at a frequency of 20 Hz in control (*Upper*) and cKO (*Lower*) mice. Arrows indicate the change induced by each AP. (*B*) Quantification of the rise in $[Na^+]_i$ associated with the AP train. Plotted are the values at the time of each AP in control (black, $n = 9$) and cKO (red, $n = 9$) mice. (*C*) The increment in $[Na^+]_i$ induced by each AP in the train in control (black) and cKO (red) mice.

other Na^+ channel subtypes. The exact molecular identity of the channels that substitute for $Na_v1.6$ in the dendrites remains elusive, however, because conventional immunofluorescence localization technique is not sufficiently sensitive.

Relatively subtle differences in excitable properties of layer 5 pyramidal neurons of conditional $Na_v1.6$ knockout and control mice, as described above, could be related to a difference between the $Na_v1.6$ and $Na_v1.2$ channels in their propensity to enter the noninactivating gating mode and to produce persistent current (9, 11, 12). Several groups have tried to determine the role of $Na_v1.6$ channels in axonal excitability by using mice that bear the recessive muscle endplate disease mutation in the *Scn8a* gene. This mutation causes the expression of a truncated nonfunctional form of $Na_v1.6$ by altering mRNA splicing due to insertion of a LINE element in exon 2 (43). The functional consequences of $Na_v1.6$ deletion varied in different neuronal types, probably reflecting differences in $Na_v1.6$ subcellular localization and time course of developmental appearance, as well as mechanisms compensating for the lack of its expression (44). Thus, the amplitude and voltage dependence of both transient and persistent Na^+ currents in dissociated globus pallidus neurons were not affected by $Na_v1.6$ deletion (45). By contrast, transient Na^+ current in dissociated Purkinje neurons and in subthalamic nucleus neurons from mutant mice with ubiquitous $Na_v1.6$ deficiency was reduced by ~40% (36, 46–48), and I_{NaP} reduction was even more prominent [by ~60% (36)]. I_{NaP} was also significantly reduced in CA1 pyramidal cells from $Na_v1.6$ KO mice, and the voltage dependence of activation of the transient current was shifted to more depolarizing potentials by ~5 mV (49). Current-clamp recordings from these cells in slices revealed a significant elevation of the somatic spike threshold in $Na_v1.6$ KO mice as well as a shortening of the estimated delay

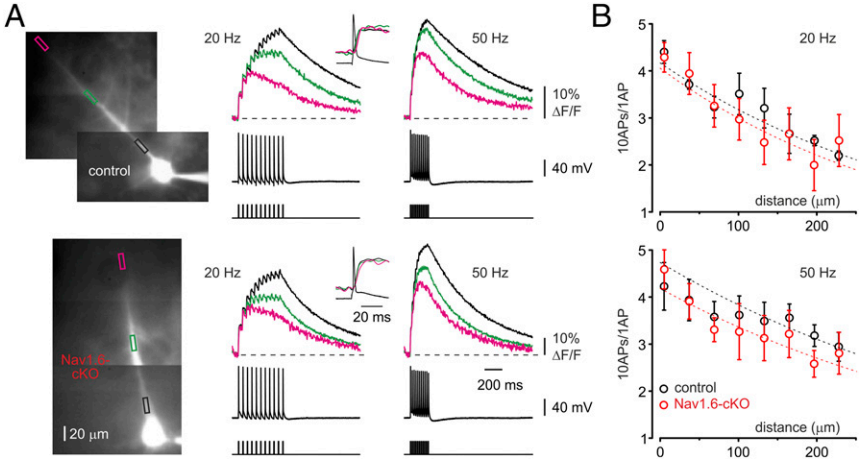

Fig. 7. Propagation efficiency of AP trains in apical dendrites is not affected by $Na_v1.6$ loss. (*A*) Ca^{2+} transients elicited in apical dendrites of the representative control (*Upper*) and $Na_v1.6$-cKO (*Lower*) neurons by trains of 10 APs at frequencies of 20 and 50 Hz. Color of the traces indicates distance from the soma (black: 25 μm; green: 125 μm: pink: 225 μm). (*Insets*) Ca^{2+} transients evoked by a single AP. (*B*) The ratio of the peak amplitude of Ca^{2+} transients elicited by a train and single APs plotted as a function of distance from the soma. The dashed lines are an exponential fit to the data. Note that in both control ($n = 7$) and $Na_v1.6$-cKO ($n = 11$) neurons, Ca^{2+} transients attenuate with a distance constant of ~360 μm (20-Hz train) and ~450 μm (50-Hz train).

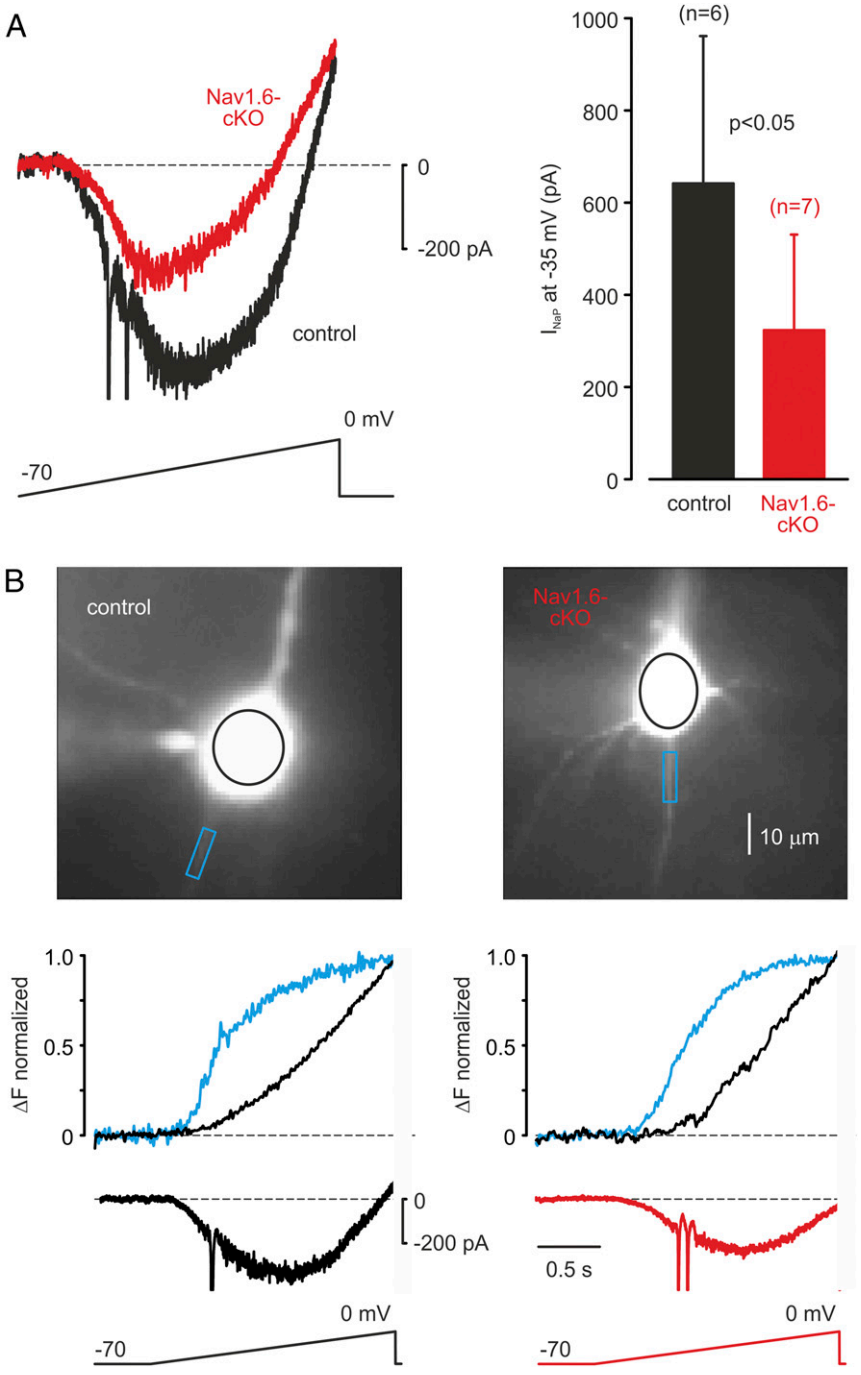

Fig. 8. Loss of $Na_v1.6$ channels reduces the magnitude, but has little effect on the voltage dependence of persistent Na^+ current. (*A*, *Left*) Superimposed I_{NaP} elicited by slow (35 mV/s) voltage ramps in a representative control (black) and cKO (red) neuron. (*A*, *Right*) Mean I_{NaP} amplitude at −35 mV is significantly reduced in cKO neurons. (*B*) Normalized ΔF transients in AIS (blue) and soma (black) elicited by 2-s-long voltage ramps from −70 to 0 mV in representative control (*Left*) and cKO (*Right*) neurons. Note that in both control and cKO neurons the AIS optical signal began to change at significantly more negative voltages as compared with the signal in the soma.

between spike initiation at the AIS and its arrival at the soma (49). These earlier studies were based on somatic electrical recordings alone. Here, using a more direct approach, Na^+ imaging from axons of current- and voltage-clamped layer 5 cortical pyramidal cells, we found that neuron-specific deletion of $Na_v1.6$ causes significant reduction in I_{NaP} generation by AIS Na^+ channels. Similarly, a heightened tendency to generate I_{NaP} was found in studies of heterologously expressed Na^+ channels, which consistently show that the noninactivating component is largest in $Na_v1.6$ channels (9, 11, 12). Because of the pivotal role of I_{NaP} in setting the AP threshold, the reduction in this current amplitude alone could be sufficient to explain elevation in current and voltage threshold and the lower instantaneous firing rates observed in $Na_v1.6$-cKO cells.

Based on the similar pattern of Na^+ influx in $Na_v1.2$ and $Na_v1.6$ containing AIS of the $Na_v1.6$-cKO and control neurons, we presume that the underlying channel densities are not dramatically different. The precise relationship between Na^+ influx and Na^+

conductance (gNa) is not simple, as it depends not only on channel kinetics but also on the shape of the AP. In an extreme example, the relationship could be quite flat in a spherical compact cell if all of the Na^+ conductance is inactivated by the time the AP reaches its peak. However, as has been shown experimentally (50, 51), rapidly rising, narrow APs such as those of the AIS at 22 °C have considerable Na^+ conductance during the repolarization phase. In this case, the influx more closely mirrors gNa. Kole et al. (14) used models with different Na^+ channel densities to show that the influx–gNa relationship is expected to be nearly linear for a fairly broad range of gNa. The Na^+ influx–gNa relationship could be significantly distorted if the inactivation kinetics of $Na_v1.2$ and $Na_v1.6$ channels differs. Our imaging data, however, suggest that this is not the case, as the kinetics of cumulative inactivation of axonal Na^+ flux during high-frequency trains of spikes was roughly similar in cKO and control cells.

A common supposition is that the leftward shift in voltage dependence of Na^+ channel activation in the AIS is due to the presence of the molecularly distinct Na^+ channel subtype, $Na_v1.6$. The comparison of the voltage dependence of the heterologously expressed $Na_v1.6$ channels to other subtypes, however, has produced conflicting results: there are reports of leftward shifted (9), rightward shifted (10), and unaffected (11) voltage dependence of activation of $Na_v1.6$ compared with $Na_V1.2$ channels. Our evidence—that the leftward shift of activation of the Na^+ channels is preserved within the $Na_v1.2$-containing AIS trigger zone of $Na_v1.6$-cKO neurons—indicates that the leftward shift is not associated with a unique channel subtype. Rather, it probably reflects interactions of Na^+ channels with the proteins that characterize the AIS (52). Indeed, the binding of one of the AIS cytoskeletal proteins, ankyrin G (31, 53), to sodium channels can regulate their inactivation gating (54).

In good agreement with our data, excitatory cell-specific deletion of $Na_v1.6$ has recently been shown to produce convulsive seizure resistance due to cortical circuit hypoexcitability (55). Examination of heterozygous $Na_v1.6$ mutant mice (56) and humans (57) revealed a much more complex phenotype than we observed, including cognitive deficits, emotional instability, sleep–wake architecture, and other neurohumoral derangements. Although these phenomena could be related to a mild decrease in neuronal excitability of various neuronal populations, it is more likely that they reflect a difference in susceptibility of different Na^+ channel subtypes to neuromodulation. For example, while somatodendritic $Na_v1.2$ channels are very sensitive to regulation by protein phosphorylation via the PKA and PKC pathways (58–60), the $Na_v1.6$ channels are largely refractory to such neuromodulation (11). It is therefore likely that compartmentalization of $Na_v1.2$ and $Na_v1.6$ channels in mature cortical neurons contributes to the selectivity of neuromodulation of the excitable properties of the axonal and somatodendritic membrane.

Materials and Methods

Ethics Statement. This study was carried out at the University of Saarland and the Max Planck Institute of Experimental Medicine in strict accordance with the recommendations of European and German guidelines for the welfare of experimental animals. Animal experiments were approved by the German Federal States of Saarland and Lower Saxony. Mouse breeding was performed in the animal facilities of the University of Saarland and Max Planck Institute for Experimental Medicine.

Generation of Transgenic Mice. The mice were of C57BL/6NRj background. Transgenic mice *Scn8a*^{tm1Mm} (29) were crossbred with Neurod6$^{tm1(cre)Kan}$ mice (26). Homozygous, floxed *Scn8a* allele mice positive for cre were used as knockouts while littermates (homozygous, floxed *Scn8a* allele but negative for cre or heterozygous, floxed *Scn8a* allele with cre) were used as control animals. Mice of both genders were investigated without obvious differences.

Immunohistochemistry. Mice (P25 and P60) were deeply anesthetized by injection of ketamine (1.4%) and xylazine (0.2%; 5 mL/kg body weight) and perfused intracardially with 2% paraformaldehyde in 0.1 M phosphate buffer (pH 7.4). After perfusion, the brains were harvested and post fixed in the same fixative solution for 2 h at room temperature (RT). Brains were washed with PBS and cut with a vibratome (Leica VT 1000S; Leica Instruments) to prepare free-floating 40-μm-thick brain slices. Frontal sections were collected and treated with blocking solution (0.3% Triton X-100 and 5% horse serum in PBS) for 1 h at RT. Primary antibodies were diluted in blocking solution. Brain slices were incubated with primary antibodies for a minimum of 12 h at 4 °C and washed with PBS after the incubation. Fluorescently tagged secondary antibodies were diluted in blocking solution, and slices were incubated for 1 h at RT. The primary antibodies used were as follows: monoclonal mouse anti-Ankyrin G (AnkG, sc-12719, 1:50; Santa Cruz Biotechnology), polyclonal rabbit anti-$Na_v1.2$ (ASC-002, 1:100; Alomone), and polyclonal rabbit anti-$Na_v1.6$ (ASC-009, 1:100; Alomone). Donkey anti-mouse or rabbit secondary antibodies (1:2,000) conjugated with Alexa488 or Alexa555 were purchased from Invitrogen.

Confocal Laser-Scanning Microscopy and Image Analysis. Confocal images were taken with a laser-scanning fluorescence microscope (LSM-710; Zeiss) using appropriate excitation and emission filters. Z-stacks of images were taken at 0.5- to 1-μm intervals, processed with ZEN software (Zeiss) and Image J, and displayed as maximum intensity projections. For counting the AISs in adult mice (Fig. 1), at least five animals per group were examined; for P25 mice, immunosections were studied from one $Na_v1.6$-cKO and one control mouse. For the analysis of AIS density and length, three to six z-stacks were taken randomly from the layer 5 cortical area of $Na_v1.2$, $Na_v1.6$, and AnkG immunostained sections. For analysis of AIS cross sections, a custom-made ImageJ plugin LRoi (available at sites.imagej.net/CIPMM-MolPhys/) was used, where the fluorescence intensity was measured along the axis perpendicular to the middle of the AIS (±2.5 μm to the right and left side) to visualize the intensity of $Na_v1.6$ and $Na_v1.2$ immunofluorescense.

Statistical Analysis. Statistical differences were analyzed using the Mann–Whitney *U* test (Na_v expression in AIS and AIS length), the two-tailed *t* test for two-group data, and the one-way Anova for three-group data. Data are shown as mean ± SEM.

Electrophysiology. Experiments were performed on L5 pyramidal neurons in somatosensory neocortical coronal slices prepared from 4- to 5-wk-old mice, using standard techniques as previously described (27). Mice were anesthetized with isoflurane (5%) and decapitated. Coronal slices (300 μm) from the primary somatosensory cortex were cut on a vibratome (VT1200; Leica) and placed in a holding chamber containing oxygenated artificial cerebrospinal fluid (ACSF) at room temperature; they were transferred to a recording chamber after more than 1 h of incubation. The composition of the ACSF was (in micromolar): 124 NaCl, 3 KCl, 2 $CaCl_2$, 2 $MgSO_4$, 1.25 NaH_2PO_4, 26 $NaHCO_3$, and 10 glucose; pH was 7.4 when bubbled with 95% O_2/CO_2.

The cells were viewed with a 63× water-immersion lens in a Zeiss Axioskop 2 FS microscope (Zeiss) mounted on an X–Y translation stage (Luigs & Neumann). Somatic whole-cell recordings were made using patch pipettes pulled from thick-walled borosilicate glass capillaries (1.5-mm outer diameter; Hilgenberg). The pipette solution contained (in micromolar): 130 K–gluconate, 6 KCl, 2 $MgCl_2$, 4 NaCl, and 10 Hepes, with pH adjusted to 7.25 with KOH. Pipettes had resistances of 5–7 MΩ when filled with this solution supplemented with 2 mM SBFI or with 50 μM OGB-1 (Molecular Probes). Current-clamp recordings were made using an EPC10 amplifier (HEKA) controlled with Patchmaster software; data were low-pass–filtered at 30 kHz (−3 dB, six-pole Bessel filter) and digitized at 200 kHz. The pipette solution for whole-cell voltage-clamp experiments contained (in micromolar): 135 CsCl, 4 NaCl, 2 $MgCl_2$, and 10 Hepes (cesium salt), pH 7.25, also supplemented with 2 mM SBFI; Ca^{2+} currents were blocked by adding 200 μM Cd^{2+} to the bath. Voltage-clamp recordings were made with an EPC10 amplifier in voltage-clamp mode; data were low-pass–filtered at 2 kHz (−3 dB, six-pole Bessel filter) and sampled at 10 kHz. Care was taken to maintain membrane access resistance as low as possible (usually 3–4 MΩ and always less than 7 MΩ); series resistance was 90% compensated for using the built-in circuitry of the amplifier.

All recordings were made at room temperature (21 ± 1 °C). We opted for a lower than physiological temperature to enhance the Na^+ transients (17). Electrophysiological data analysis was accomplished using pCLAMP 10.0 (Axon Instruments) and Origin 6.0 (Origin Lab).

Imaging. Imaging experiments were performed as described previously (17). SBFI fluorescence was excited with a 75-W Xenon arc lamp using a Semrock Fura-2 filter set [excitation = 387(11) nm; dichroic (DC) = 409 nm; emission (EM) = 510(84) nm]. OGB-1 fluorescence was excited with a high-intensity

LED device (480 ± 5 nm, Prizmatix), and the emission was collected using a modified Zeiss GFP filter set (DC = 510 nm; EM = 515 nm). Changes in fluorescence were acquired using a back-illuminated 80- × 80-pixel cooled camera (NeuroCCD-SMQ; RedShirt Imaging) controlled by the Neuroplex software. Images were acquired at 500 frames per second. Indicator bleaching was corrected by subtracting an equivalent trace without electrical stimulation.

ACKNOWLEDGMENTS. We thank M. Meisler for providing floxed *Scn8a* ($Na_v1.6$) mice; Gebhard Stopper for writing the LRoi ImageJ plugin; and Daniel Rhode for animal husbandry. This research was supported by a grant from the German–Israeli Foundation for Scientific Research and Development (to M.J.G., F.W., and I.A.F.); by Grant 1302/14 from the Israel Science Foundation (to I.A.F.); by Deutsche Forschungsgemeinschaft (DFG) Grant Programs Priority Programme 1172, Collaborative Research Center (CRC) 1757, CRC 894, and Research Unit 2289 (F.K.); and European Commission (EC) Grant Agreement FP7-202167 NeuroGLIA (to F.K.). Furthermore, the work was partially supported by the Federal Ministry for Education and Research under Grant 01GQ1005B by DFG CRC 889, and by VolkswagenStiftung under Grant ZN2632 (to F.W.).

1. Bean BP (2007) The action potential in mammalian central neurons. *Nat Rev Neurosci* 8:451–465.
2. Kole MH, Stuart GJ (2012) Signal processing in the axon initial segment. *Neuron* 73: 235–247.
3. Bender KJ, Trussell LO (2012) The physiology of the axon initial segment. *Annu Rev Neurosci* 35:249–265.
4. Goldin AL, et al. (2000) Nomenclature of voltage-gated sodium channels. *Neuron* 28: 365–368.
5. Lorincz A, Nusser Z (2008) Cell-type-dependent molecular composition of the axon initial segment. *J Neurosci* 28:14329–14340.
6. Hu W, et al. (2009) Distinct contributions of Na(v)1.6 and Na(v)1.2 in action potential initiation and backpropagation. *Nat Neurosci* 12:996–1002.
7. Li T, et al. (2014) Action potential initiation in neocortical inhibitory interneurons. *PLoS Biol* 12:e1001944.
8. Tian C, Wang K, Ke W, Guo H, Shu Y (2014) Molecular identity of axonal sodium channels in human cortical pyramidal cells. *Front Cell Neurosci* 8:297.
9. Rush AM, Dib-Hajj SD, Waxman SG (2005) Electrophysiological properties of two axonal sodium channels, Nav1.2 and Nav1.6, expressed in mouse spinal sensory neurones. *J Physiol* 564:803–815.
10. Zhou W, Goldin AL (2004) Use-dependent potentiation of the Nav1.6 sodium channel. *Biophys J* 87:3862–3872.
11. Chen Y, et al. (2008) Functional properties and differential neuromodulation of Na(v)1.6 channels. *Mol Cell Neurosci* 38:607–615.
12. Smith MR, Smith RD, Plummer NW, Meisler MH, Goldin AL (1998) Functional analysis of the mouse Scn8a sodium channel. *J Neurosci* 18:6093–6102.
13. Colbert CM, Pan E (2002) Ion channel properties underlying axonal action potential initiation in pyramidal neurons. *Nat Neurosci* 5:533–538.
14. Kole MH, et al. (2008) Action potential generation requires a high sodium channel density in the axon initial segment. *Nat Neurosci* 11:178–186.
15. Stuart G, Sakmann B (1995) Amplification of EPSPs by axosomatic sodium channels in neocortical pyramidal neurons. *Neuron* 15:1065–1076.
16. Astman N, Gutnick MJ, Fleidervish IA (2006) Persistent sodium current in layer 5 neocortical neurons is primarily generated in the proximal axon. *J Neurosci* 26: 3465–3473.
17. Fleidervish IA, Lasser-Ross N, Gutnick MJ, Ross WN (2010) Na+ imaging reveals little difference in action potential-evoked Na+ influx between axon and soma. *Nat Neurosci* 13:852–860.
18. Crill WE (1996) Persistent sodium current in mammalian central neurons. *Annu Rev Physiol* 58:349–362.
19. Vervaeke K, Hu H, Graham LJ, Storm JF (2006) Contrasting effects of the persistent Na+ current on neuronal excitability and spike timing. *Neuron* 49:257–270.
20. Mainen ZF, Joerges J, Huguenard JR, Sejnowski TJ (1995) A model of spike initiation in neocortical pyramidal neurons. *Neuron* 15:1427–1439.
21. Eyal G, Mansvelder HD, de Kock CP, Segev I (2014) Dendrites impact the encoding capabilities of the axon. *J Neurosci* 34:8063–8071.
22. Gulledge AT, Bravo JJ (2016) Neuron morphology influences axon initial segment plasticity. *eNeuro* 3:ENEURO.0085-15.2016.
23. Telenczuk M, Fontaine B, Brette R (2017) The basis of sharp spike onset in standard biophysical models. *PLoS One* 12:e0175362.
24. Burgess DL, et al. (1995) Mutation of a new sodium channel gene, Scn8a, in the mouse mutant 'motor endplate disease'. *Nat Genet* 10:461–465.
25. Susuki K, Rasband MN (2008) Molecular mechanisms of node of Ranvier formation. *Curr Opin Cell Biol* 20:616–623.
26. Goebbels S, et al. (2006) Genetic targeting of principal neurons in neocortex and hippocampus of NEX-Cre mice. *Genesis* 44:611–621.
27. Baranauskas G, David Y, Fleidervish IA (2013) Spatial mismatch between the Na+ flux and spike initiation in axon initial segment. *Proc Natl Acad Sci USA* 110:4051–4056.
28. Boiko T, et al. (2003) Functional specialization of the axon initial segment by isoform-specific sodium channel targeting. *J Neurosci* 23:2306–2313.
29. Levin SI, Meisler MH (2004) Floxed allele for conditional inactivation of the voltage-gated sodium channel Scn8a (NaV1.6). *Genesis* 39:234–239.
30. Kordeli E, Lambert S, Bennett V (1995) AnkyrinG. A new ankyrin gene with neural-specific isoforms localized at the axonal initial segment and node of Ranvier. *J Biol Chem* 270:2352–2359.
31. Galiano MR, et al. (2012) A distal axonal cytoskeleton forms an intra-axonal boundary that controls axon initial segment assembly. *Cell* 149:1125–1139.
32. Coombs JS, Curtis DR, Eccles JC (1957) The generation of impulses in motoneurones. *J Physiol* 139:232–249.
33. Kuba H, Oichi Y, Ohmori H (2010) Presynaptic activity regulates Na(+) channel distribution at the axon initial segment. *Nature* 465:1075–1078.
34. Grubb MS, Burrone J (2010) Activity-dependent relocation of the axon initial segment fine-tunes neuronal excitability. *Nature* 465:1070–1074.
35. Connors BW, Gutnick MJ (1990) Intrinsic firing patterns of diverse neocortical neurons. *Trends Neurosci* 13:99–104.
36. Raman IM, Sprunger LK, Meisler MH, Bean BP (1997) Altered subthreshold sodium currents and disrupted firing patterns in Purkinje neurons of Scn8a mutant mice. *Neuron* 19:881–891.
37. Aman TK, Raman IM (2007) Subunit dependence of Na channel slow inactivation and open channel block in cerebellar neurons. *Biophys J* 92:1938–1951.
38. Lorincz A, Nusser Z (2010) Molecular identity of dendritic voltage-gated sodium channels. *Science* 328:906–909.
39. Spruston N, Schiller Y, Stuart G, Sakmann B (1995) Activity-dependent action potential invasion and calcium influx into hippocampal CA1 dendrites. *Science* 268: 297–300.
40. Tsubokawa H, Ross WN (1997) Muscarinic modulation of spike backpropagation in the apical dendrites of hippocampal CA1 pyramidal neurons. *J Neurosci* 17: 5782–5791.
41. Jung HY, Mickus T, Spruston N (1997) Prolonged sodium channel inactivation contributes to dendritic action potential attenuation in hippocampal pyramidal neurons. *J Neurosci* 17:6639–6646.
42. Larkum ME, Kaiser KM, Sakmann B (1999) Calcium electrogenesis in distal apical dendrites of layer 5 pyramidal cells at a critical frequency of back-propagating action potentials. *Proc Natl Acad Sci USA* 96:14600–14604.
43. Kohrman DC, Smith MR, Goldin AL, Harris J, Meisler MH (1996) A missense mutation in the sodium channel Scn8a is responsible for cerebellar ataxia in the mouse mutant jolting. *J Neurosci* 16:5993–5999.
44. Van Wart A, Matthews G (2006) Impaired firing and cell-specific compensation in neurons lacking nav1.6 sodium channels. *J Neurosci* 26:7172–7180.
45. Mercer JN, Chan CS, Tkatch T, Held J, Surmeier DJ (2007) Nav1.6 sodium channels are critical to pacemaking and fast spiking in globus pallidus neurons. *J Neurosci* 27: 13552–13566.
46. Khaliq ZM, Gouwens NW, Raman IM (2003) The contribution of resurgent sodium current to high-frequency firing in Purkinje neurons: An experimental and modeling study. *J Neurosci* 23:4899–4912.
47. Do MT, Bean BP (2004) Sodium currents in subthalamic nucleus neurons from Nav1.6-null mice. *J Neurophysiol* 92:726–733.
48. Grieco TM, Raman IM (2004) Production of resurgent current in NaV1.6-null Purkinje neurons by slowing sodium channel inactivation with beta-pompilidotoxin. *J Neurosci* 24:35–42.
49. Royeck M, et al. (2008) Role of axonal NaV1.6 sodium channels in action potential initiation of CA1 pyramidal neurons. *J Neurophysiol* 100:2361–2380.
50. Carter BC, Bean BP (2009) Sodium entry during action potentials of mammalian neurons: Incomplete inactivation and reduced metabolic efficiency in fast-spiking neurons. *Neuron* 64:898–909.
51. Carter BC, Bean BP (2011) Incomplete inactivation and rapid recovery of voltage-dependent sodium channels during high-frequency firing in cerebellar Purkinje neurons. *J Neurophysiol* 105:860–871.
52. Grubb MS, et al. (2011) Short- and long-term plasticity at the axon initial segment. *J Neurosci* 31:16049–16055.
53. Zhou D, et al. (1998) AnkyrinG is required for clustering of voltage-gated Na channels at axon initial segments and for normal action potential firing. *J Cell Biol* 143: 1295–1304.
54. Shirahata E, et al. (2006) Ankyrin-G regulates inactivation gating of the neuronal sodium channel, Nav1.6. *J Neurophysiol* 96:1347–1357.
55. Makinson CD, et al. (2017) Regulation of thalamic and cortical network synchrony by Scn8a. *Neuron* 93:1165–1179.e6.
56. Papale LA, et al. (2010) Dysfunction of the Scn8a voltage-gated sodium channel alters sleep architecture, reduces diurnal corticosterone levels, and enhances spatial memory. *J Biol Chem* 285:16553–16561.
57. Trudeau MM, Dalton JC, Day JW, Ranum LP, Meisler MH (2006) Heterozygosity for a protein truncation mutation of sodium channel SCN8A in a patient with cerebellar atrophy, ataxia, and mental retardation. *J Med Genet* 43:527–530.
58. Numann R, Catterall WA, Scheuer T (1991) Functional modulation of brain sodium channels by protein kinase C phosphorylation. *Science* 254:115–118.
59. Li M, et al. (1993) Convergent regulation of sodium channels by protein kinase C and cAMP-dependent protein kinase. *Science* 261:1439–1442.
60. Cantrell AR, Catterall WA (2001) Neuromodulation of Na+ channels: An unexpected form of cellular plasticity. *Nat Rev Neurosci* 2:397–407.